J Neuropathol Exp Neurol
Vol. 72, No. 12
December 2013
pp. 1171–1181

ORIGINAL ARTICLE

Structural and Expression Differences Between the Vasculature of Pilocytic Astrocytomas and Glioblastomas

Dana Mustafa, PhD, Sigrid Swagemakers, MSci, Pim French, PhD, Theodorus M. Luider, PhD, Peter van der Spek, PhD, Andreas Kremer, MSci, and Johan M. Kros, MD, PhD

Abstract

The identification of differences in vascular architecture and utilization of angiogenic pathways is a first step for identifying specific targets for tailored antiangiogenic therapies of brain tumor patients. Here, we compared the proliferating vasculature of 2 glioma subtypes with entirely different biologic behaviors and molecular background at the immunophenotype and gene expression levels. Proliferating vessels in 13 pilocytic astrocytomas and 8 glioblastomas were compared for differences in the composition of the vascular walls using confocal microscopy for markers of endothelial cells and pericytes/mural cells. Endothelial, pericytic, and mural cells had normal-appearing arrangements in the vessels in pilocytic astrocytomas, whereas those in glioblastomas appeared to be more disorganized. In addition, differences in expression of angiogenesis-related genes were sought in the tumor specimens using RNA expression arrays. There were 114 out of 2,894 differentially expressed angiogenesis-related genes between these 2 glioma subtypes indicating differences in the utilization of various pathways. These results point to the need for detailed information on mechanisms of neoangiogenesis in tumor subtypes to facilitate the development of specific antiangiogenic strategies.

Key Words: Angiogenesis, Glioblastoma, Immunofluorescence, Pilocytic astrocytoma, RNA expression.

INTRODUCTION

Gliomas are among neoplasms with the highest degree of neovascularization. Therefore, it may be surprising that antiangiogenic agents have had only limited therapeutic success in these tumors (1, 2). The efficacy of antiangiogenic therapy improves when agents such as bevacuzimab are combined with cytostatic therapy. This might be explained by the participation of tumor cells in triggering tumor neovascularization (3). Therefore, the search for angiogenesis-related expression patterns should not be restricted only to the tumor blood vessels. To identify new targets for future angiogenic strategies, detailed knowledge of aberrant structure and functions of the tumor vessels and of differences in the utilization of angiogenic pathways in physiologic and neoplastic angiogenesis is needed.

Vascularization in tumors is triggered by hypoxia and vascular endothelial growth factor (VEGF) upregulation because of an increased demand for oxygen by rapidly growing cells. Initially, the preexisting vessels of the host are co-opted by the tumor cells, followed by the formation of new blood vessels. Vessel strands composed of single endothelial cells are dependent on VEGF expression to consolidate and escape regression (4, 5). In diffusely infiltrating gliomas, the vascular density gradually increases (6) and defective regulation of the neovascularization becomes apparent from uncontrolled proliferation of the cellular components of the vessel walls, that is, ''microvascular proliferation.'' The recruitment of pericytes and other mural cells, however, is defective, resulting in unstable vascular channels (7). The vessels ultimately progress into the dysfunctional glomeruloid and pseudosarcomatous structures that are characteristic of glioblastoma (GBM) (8). The malformed vessels are leaky, and there is disruption of the blood-brain barrier. Interestingly, microvascular proliferation also develops in pilocytic astrocytomas (PAs), which have a very different genetic background and biologic behavior (9). High cell density, high proliferation of tumor cells, and necrosis are generally absent in PAs (10, 11). In contrast to the molecular background of diffuse infiltrating gliomas, which often harbor mutations of *TP53* and *IDH1*, loss of heterozygosity for 10q, and endothelial growth factor receptor amplification, most PAs are genetically characterized by the KIAA1549-BRAF duplication insertion (12). The effects of the genetic characteristics of tumors on neoangiogenesis are largely unknown. In papillary thyroid carcinomas carrying the BRAF V600 mutation, a relationship with hypoxia inducible factor-1α (HIF-1α) expression was identified (13), but no such association with the KIAA1549-BRAF duplication insertion in PAs has been revealed. Only a few studies have focused on structural and qualitative differences between the vasculature of PA and high-grade diffusely infiltrating glioma (14).

In the present study, we sought to identify structural differences of the proliferating vessels of both glioma subtypes using multiple markers for endothelial cells, pericytes, and mural cells for analysis by confocal microscopy. At the gene expression level, we focused on angiogenesis-related

From the Departments of Pathology (DM, JMK), BioInformatics (SS, PvdS, AK), and Neurology (PF, TML), Erasmus Medical Center, Rotterdam, The Netherlands.
Send correspondence and reprint requests to: Johan M. Kros, MD, PhD, Department of Pathology, Erasmus Medical Center, Dr. Molewaterplein 50, 3000 DR Rotterdam, The Netherlands; E-mail: j.m.kros@erasmusmc.nl
No specific funding sources are to be revealed.
The authors declare that they have no conflicts of interest.

TABLE 1. Demographic Data on Tumor Patients and Controls

	Diagnosis/Cause of Death	Sex	Age, years	Tumor Location/Region Analyzed
1	PA	F	1	Cerebellum
2	PA	M	5	Cerebellum
3	PA	F	5	Cerebellum
4	PA	M	51	Cerebellum
5	PA	F	36	Cerebellum/brainstem
6	PA	F	22	Left occipital
7	PA*	F	12	Cerebellum
8	PA*	F	22	Cerebellum
9	PA*	F	24	Cerebellum
10	PA*	M	32	Cerebellum
11	PA*	M	34	Cerebellum
12	PA*	F	37	Cerebellum
13	PA*	M	16	Cerebellum / Brain stem
14	GBM*	F	63	Left frontal
15	GBM*	F	54	Left frontoparietal
16	GBM*	M	55	Right frontal
17	GBM*	M	46	Right frontoparietal
18	GBM*	F	61	Right frontal
19	GBM*	F	64	Left temporal
20	GBM*	M	67	Right temporal
21	GBM*	M	81	Left occipital
C	Myocardial infarction	M	55	Left frontal
C	Rupture aneurysm abdominal aorta	M	61	Right temporal
C	Myocardial infarction	F	44	Cerebellum
C	Pulmonary embolism	F	69	Left frontal
C	Myocardial infarction	M	41	Right frontal
C	Subarachnoid hemorrhage	M	63	Cerebellum
C	Subarachnoid hemorrhage	F	53	Right frontal

*Cases included in the expression array analysis.
C, control brain; F, female; M, male.

pathways. Comparing the structural characteristics of the vasculatures of GBM and PA and underlying angiogenesis-related RNA expression patterns may reveal differences in the utilization of molecular pathways and the underlying stimuli of neoangiogenesis.

MATERIALS AND METHODS

Patients and Tumor Samples

A total of 21 gliomas were used for this study, including 13 PAs and 8 GBMs. Ten fields harboring areas of proliferated vasculature were selected in each tumor sample by 2 authors (Johan Kros and Dana Mustafa) and used for fluorescent triple labeling. Inspection of the various single-, double-, and triple-labeled slides was performed independently by the authors. All 13 PAs contained the KIAA1549-BRAFF duplication/insertion, as tested by FISH (Kreatech Diagnostics, Amsterdam, The Netherlands). The GBMs were isocitrate dehydrogenase 1 (IDH1) wild type and did not have *TP53* mutations (primary GBM). RNA expression arrays were obtained from 7 of 13 PAs and all 8 GBMs (Table 1). In addition, formalin-fixed, paraffin-embedded samples from 7 control autopsy brains were used for single, double, and triple immunostaining (Table 1).

Immunohistochemistry

All 13 PAs and 8 GBMs were used for the immunofluorescence studies. Because cells of various lineages may take aberrant positions in the vessels walls, the inner, middle, and outer layers were evaluated as follows: the inner layer is the cell layer bordering the lumen of the vessel; the outer layer is the cell layer bordering the surrounding neuropil; and the middle layer takes the position between the inner and outer cell layer. Small vessels had 1 layer; hypertrophic and glomeruloid vessels had more than 1 layer. Glomeruloid vessels appear as nodular tufts rather than tubular structures. Markers for endothelial cells, activated endothelial cells, and pericytic/mural cells were used to characterize the cellular components of the blood vessel walls. The cellular constituents of the microvasculature of gliomas were identified as CD31-positive, CD34-positive endothelial cells; CD105-positive activated endothelial cells; NG2-positive/endosialin-positive pericytes (15–19); and α-smooth muscle actin (SMA)–positive mural cells. In previous studies, colligin 2 (heat shock protein 47), a chaperone for collagen, was found to be specific for the neovasculature of diffusely infiltrating gliomas as opposed to vasculature of normal brain (20, 21).

In addition, immunostaining for VEGF-A and HIF-1α was performed on adjacent slides of the selected areas. All

TABLE 2. Antibodies

Antibody/Antigen	Dilution	Commercial Source
Monoclonal colligin 2	1:500	Stressgen, Ann Arbor, MI
Polyclonal colligin 2	1:100	MBL international, Woburn, MA
CD31	1:40	Dako, Glostrup, Denmark
CD34	1:30	Dako
CD105	1:2000	Dako
NG2	1:100	ZYMED Laboratories, South San Francisco, CA
Endosialin	1:500	Prof. C. Isacke, Institute of Cancer Research, London, UK
αSMA	1:40	Biogenex, San Ramon, CA
Collagen type IV	1:25	Dako
VEGF-A	1:200	Santa Cruz Biotechnology, Santa Cruz, CA
HIF-1α	1:100	BD Bioscience, San Jose, CA
Cy3 goat anti-rabbit	1:100	BioLegend, San Diego, CA
Biotin–horse–anti-mouse	1:200	Vector Laboratories, Inc., Peterborough, UK
FITC-conjugated avidin	1:50	Jackson ImmunoResearch, West Grove, PA
Cy5-conjugated donkey anti-rabbit	1:50	Jackson ImmunoResearch
Cy3 goat anti-mouse antibody	1:100	BioLegend

immunostained sections (immunofluorescence and light microscopy) were evaluated by 2 observers (Johan Kros and Dana Mustafa). The mean of percentages of positive cells was determined.

Single Staining

Adjacent sections of 5-μm thickness were used for immunohistochemical comparisons. All antibodies used and their specifications are listed in Table 2. Staining procedures were as reported previously (20). Immunohistochemical staining was performed following the manufacturer's instructions (alkaline phosphatase technique). The sections were deparaffinized in xylene for 15 minutes and rehydrated through graded alcohols and washed with water and with PBS. The sections were then incubated with the specific antibodies for 30 minutes. After washing with PBS, the corresponding secondary antibody was added and incubated for 30 minutes at room temperature. Fuchsin Alkaline Phosphatase Substrate Solution (Dako, Glostrup, Denmark) was freshly prepared, and the sections were then incubated for about 30 minutes, washed with tap water, counterstained, and coverslipped with permanent mounting medium.

Double Staining

Double immunolabeling for colligin 2 and the various markers for endothelial cells and pericytes was performed as previously described (20). Adjacent 5-μm-thick slides of tissue samples were mounted onto noncoated microscope slides, fixed in acetone for 15 minutes, and air-dried. Sections were incubated with anti–colligin 2 polyclonal antibody for 30 minutes, washed, and incubated with Cy3-conjugated goat anti-rabbit immunoglobulin for 30 minutes. After washing, sections were incubated with the second monoclonal antibody for 30 minutes, followed by 30 minutes of labeling with biotin–horse–anti-mouse antibody. The fluorescein isothiocyanate (FITC)– conjugated avidin method was used for detection. Nuclei were counterstained with 4′,6-diamidino-2-phenylindole (DAPI) in a vector sheet (1:1000). All antibodies were also used in single staining procedures to ensure the specificity of the antibody; negative controls included the secondary antibody alone for both single and double staining procedures.

Triple Staining

In triple immunolabeling, immunohistochemistry for colligin 2 and CD31 was combined with markers for activated endothelial cells (CD105), for pericytes (NG2; endosialin), or for other mural cells (SMA). The 6 frozen biopsy samples of PAs were used for the triple staining. Adjacent slides of 5-μm-thick sections were mounted onto noncoated microscope slides, fixed in acetone for 15 minutes, and air-dried. Sections were incubated with anti–colligin 2 polyclonal antibody for 30 minutes, washed, and incubated again with Cy5-conjugated donkey anti-rabbit for 30 minutes. After washing, sections were incubated with the monoclonal antibody to CD105, SMA, NG2, or endosialin, then washed and incubated with biotin-labeled horse anti-mouse antibody. Fluorescein isothiocyanate–conjugated avidin was used for detection. After washing, sections were incubated with anti-CD31 and anti-colligin 2 monoclonal antibody for 30 minutes, followed by 30 minutes of labeling with Cy3-conjugated goat anti-mouse antibody. After washing, nuclei were counterstained with DAPI, as above, and the slides were then coverslipped. Staining controls were as previously described.

Confocal Laser Scanning Microscopy

Confocal images of double- and triple-stained sections were obtained using a confocal laser scanning microscope (LSM510; Carl Zeiss MicroImaging, Jena, Germany) equipped with a Plan-Neofluar 40×/1.3 NA oil objective (Carl Zeiss MicroImaging). A diode laser was used for excitation of DAPI at 405 nm, an argon laser for FITC at 488 nm, a HeNe-laser for Cy3 at 543 nm, and a HeNe-laser for Cy5 at 633 nm. For DAPI, an emission bandpass filter of 420 to 480 nm; for FITC, a bandpass filter of 500 to 530 nm; for CY3, a bandpass filter of 560 to 615 nm; and for Cy5, a longpass filter of 650 nm

TABLE 3. Immunohistochemical Marker Analysis of the Cellular Components of the Neovasculature in Pilocytic Astrocytomas and Glioblastomas

			Endothelial Cells			Pericytes		Mural Cells		All Cells
Blood Vessel Type	Glioma Type	Layers	CD31	CD34	CD105	Endosialin	NG2	αSMA	Collagen Type IV	Colligin 2
Small, normal-looking vessels	PA	Single	+	+	+	+	+	+	+	+
	GBM	Single	+	+	+	+	+	+	-	+
Hypertrophied vessels	PA	Inner	+	+	+	-	-	-	-	+
		Middle	-	-	-	+	+	+	+	+
		Outer	-	-	-	+	+	+	+	+
	GBM	Inner	+*	+	+	+*	+	-	-	+
		Middle	+	+	+	+	+	+	-	+
		Outer	+	+	+	+	+	+	+	+
Glomeruloid vessels	PA	Inner	+	+	+	-	-	-	-	+
		Outer	-	+	-	+	+	+	+	+
	GBM	Inner	+	+	+	+	+	+	-	+
		Outer	+	+	+	+	+	+	+	+

The endothelial, pericytic, and mural cells were characterized by immune reactivity for the antigens listed.
*The indicated patterns are representative of the majorities of the evaluated blood vessels.
+, present; -, absent.

were used. The signals were recorded sequentially (multitrack option) to avoid crossing over of the signals, and data were stored in separate channels.

RNA Expression Profiles and Pathway Analysis

Because angiogenesis-related molecules are not only expressed by cells constituting the vessel walls but also by surrounding cells (i.e. glial cells, endothelial progenitor cells, and microglia), whole tissue sections were used for the expression arrays. The procedure of nucleic acid isolation, cDNA synthesis, and array hybridization was reported previously by Gravendeel et al (22). Total RNA and genomic DNA were isolated from 20 to 40 cryostat sections of 40-μm thickness using Trizol (Invitrogen, Billerica, MA) according to the manufacturer's instructions (23) and further purified on RNeasy mini columns (Qiagen, Valencia, CA). RNA quality was assessed on a Bioanalyzer (Agilent Technologies, Santa Clara, CA). High-quality RNA (1–2 μg; RNA integrity number >6.5 [24]) was used. Double-stranded cDNA synthesis and labeled cRNA synthesis were performed according to the Affymetrix Eukaryotic One-cycle cDNA synthesis protocol (Affymetrix, Santa Clara, CA). Affymetrix HU133 Plus 2.0 microarrays were hybridized overnight with 10 μg of biotin-labeled cRNA. Gene chips with a glyceraldehyde-3-phosphate dehydrogenase 5′/3′ ratio greater than 4, present calls less than 30%, unsuccessful room temperature controls, or a background greater than 200 were excluded. Robustness of sample processing was assessed using 8 biologic replicates and 3 technical replicates. Replicates were not included in any analysis. Sample labeling and array hybridization on 250K *Nsp*I arrays were performed using high-quality genomic DNA according to the Genechip Mapping 500K Assay Manual (n = 40) (Affymetrix). Sample labeling and array hybridization on single-nucleotide polymorphism 6.0 arrays were performed using Trizol-extracted, Repli-G (Qiagen)–amplified genomic DNA by AROS Applied Biotechnology AS according to standard Affymetrix protocols (n = 15).

Raw intensity values of all samples were normalized by Robust Multichip Analysis normalization, including background correction and quantile normalization using the Partek version 6.5 (Partek Inc., St. Louis, MO). The normalized data file was transposed and imported into OmniViz version 6.0.1 (BioWisdom Ltd., Cambridge, UK) for further analysis. For each probe set, the geometric mean of the hybridization intensity of all samples was calculated. The level of expression of each probe set was determined relative to this geometric mean and ^{2}log-transformed. The geometric mean of the hybridization signal of all samples was used to ascribe equal weight to gene expression levels with similar relative distances to the geometric mean. Differentially expressed genes were identified using statistical analysis of microarrays. Cutoff values for significantly expressed genes were a false discovery rate of 0.01 or less and a fold change of 1.5. Functional annotation of the statistical analysis of microarrays results was done using Ingenuity Pathway Analysis (Ingenuity, Mountain View, CA).

RESULTS

Comparison of the Vasculature of PA and GBM

All vessels in 10 representative fields of the tumor specimens were examined, and vessels of similar sizes in both glioma subtypes were characterized by immunohistochemistry and compared by 2 observers (Johan Kros and Dana Mustafa). The results of the analysis by confocal microscopy of the immunofluorescent multilabeling are summarized in Table 3. In line with previous investigations (21), colligin 2 expression was present in all vessel subtypes, including newly formed vessels, and in all cells constituting the blood vessels in PAs and GBMs (Figs. 1–4). The distribution of the cells with the respective endothelial, pericytic, or mural lineages within the inner, middle, and outer layers of the hypertrophied/glomeruloid vessels differed between the 2 glioma subtypes (Table 3; Figs. 2, 3). In hypertrophic and

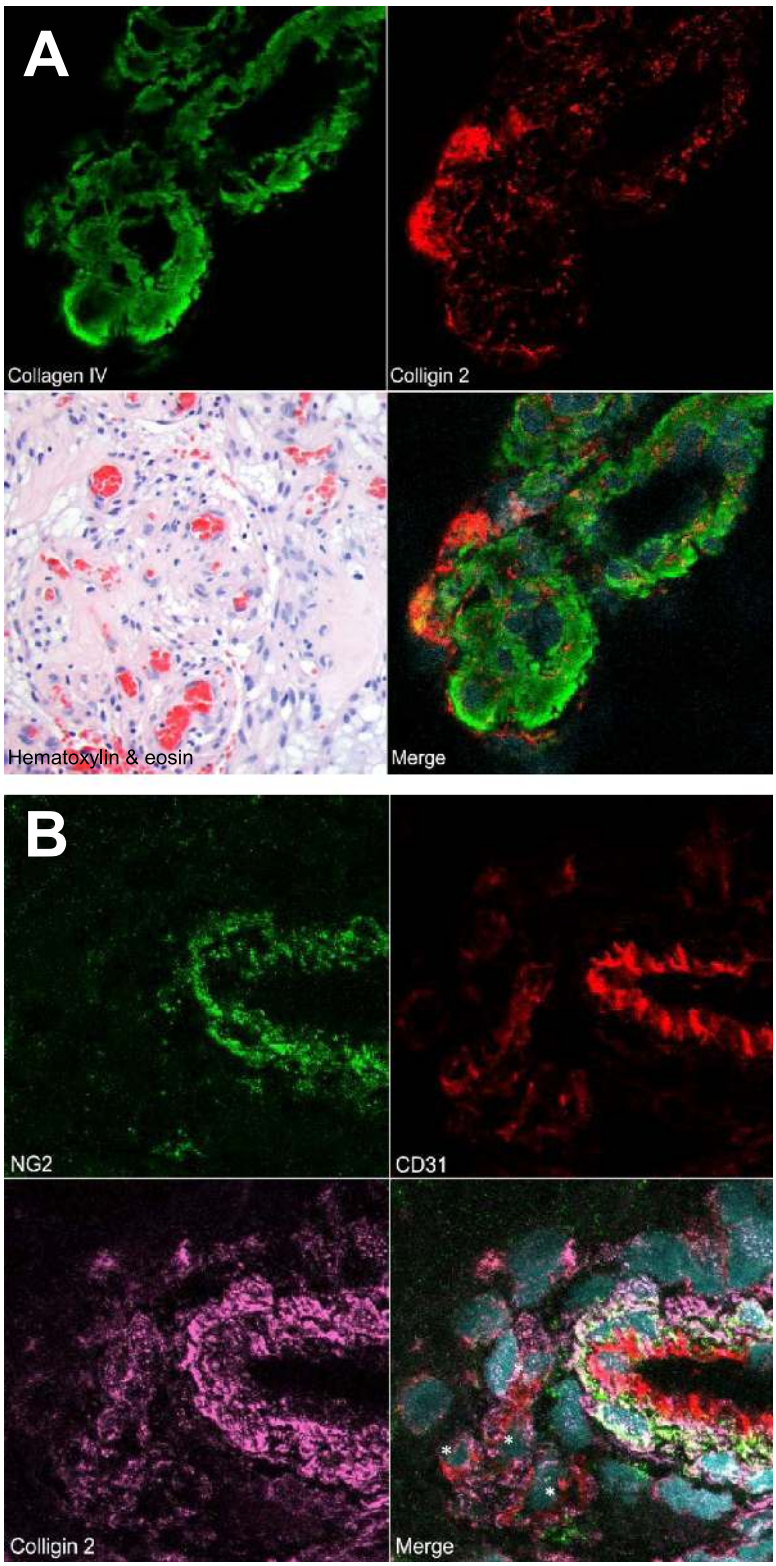

FIGURE 1. Hypertrophic vessels in pilocytic astrocytoma (PA). **(A)** Hypertrophic vessels in a PA (Case 7) immunostained for collagen type IV and colligin 2. Colligin 2 is expressed ubiquitously in all tumor vessels. There is abundant expression of collagen type IV (original magnification = 200×; lower left panel light microscopy; upper panels and lower right panel confocal microscopy; DAPI counterstain in merged panel lower right). **(B)** The structure of the vessel wall is essentially intact; the outer layer of NG2-positive pericytes covers an inner layer of CD31-positive endothelial cells (confocal microscopy; original magnification = 400×; DAPI counterstain in lower right panel).

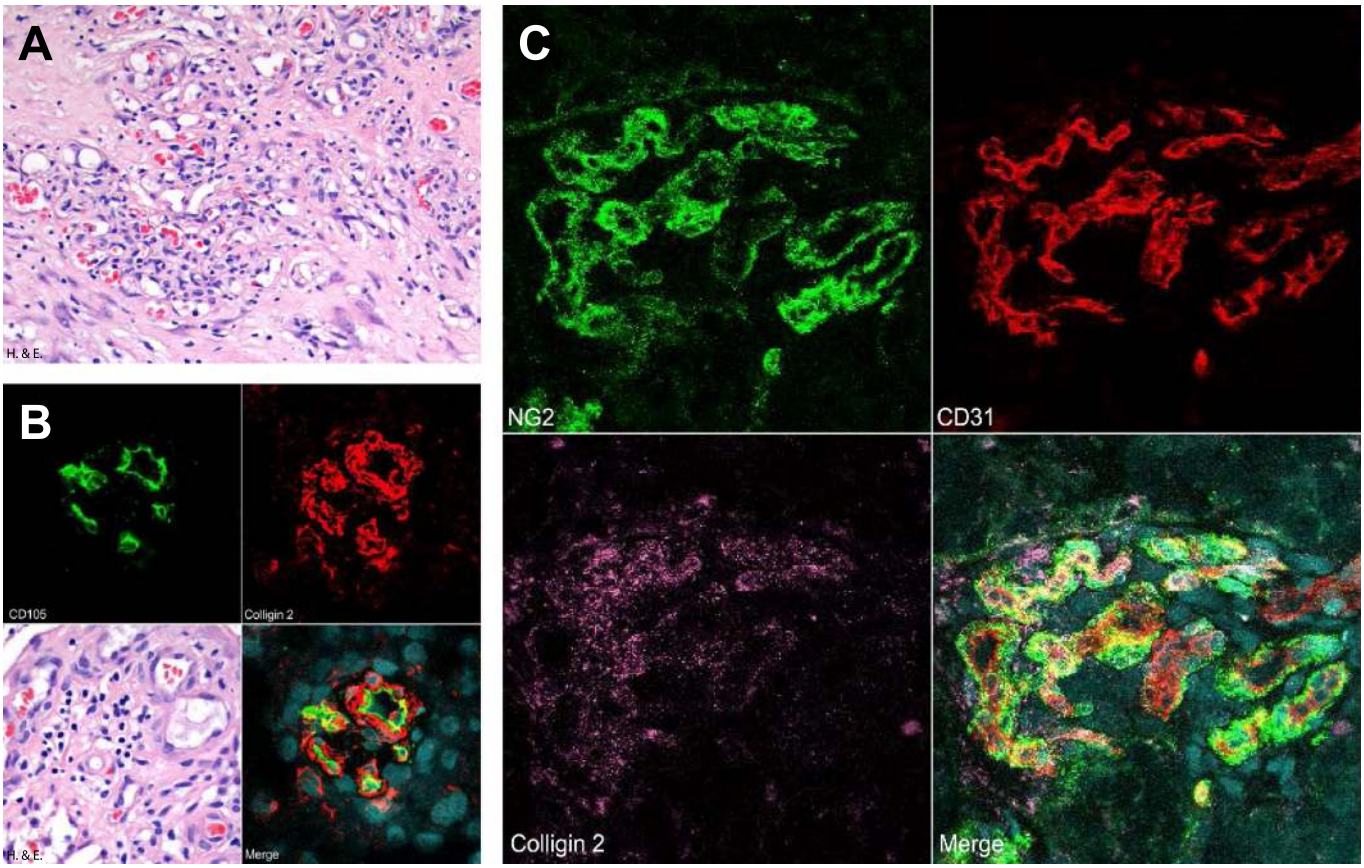

FIGURE 2. Glomeruloid vessels in pilocytic astrocytoma (PA). **(A)** Glomeruloid vessels contain many lumina giving a telangiectatic appearance (light microscopy, original magnification = 200×). **(B)** The walls of glomeruloid vessels in PA (Case 9) show orderly layering. There is an inner layer of CD105-positive (activated) endothelial cells. All layers express colligin 2 (lower left panel light microscopy; upper panels and lower right panel confocal microscopy; original magnification = 200×; DAPI counterstain in merged panel lower right). **(C)** The intact layering is illustrated by an inner lumen-lining layer of CD31-positive endothelial cells and expression of the pericytic marker NG2 in the outer layers. Colligin 2 is expressed throughout the vessel wall (confocal microscopy; original magnification = 100×; DAPI counterstain in merged panel lower right). Hematoxylin and eosin stain.

glomeruloid vessels of PAs, there were increased cell numbers, but the relative position of the endothelial, pericytic, and mural cells remained intact. Unlike in GBMs, endothelial cells in the PAs were confined to the inner layer of the hypertrophied and glomeruloid vessels (Figs. 2B, C; 4B). NG2-positive/endosialin -positive pericytes are found in the inner layers of the hypertrophied and glomeruloid vessels of the GBMs, but not in these vessels of the PAs (Figs. 1B; 2C; 3; 4B, C). Another distinction between the vasculature of GBM and PA was the paucity of thrombotic and recanalized vessels in the latter. The small vessels of the PAs are immunopositive for collagen type IV (Fig. 1), whereas similar vessels in GBM lacked expression of collagen type IV.

The expression of VEGF-A and HIF-1α varied in both PAs and GBMs; both were higher in the GBMs than in the PAs. A mean of 40% (36–45%) VEGF-A positive cells were identified in all GBMs; 40% of cells were positive (mean of 36% and 45%). In all PAs, VEGF-A–immunopositive cells were present, and the mean percentage was 20% (20% and 20% for the 2 observers). Hypoxia inducible factor-1α immunopositivity was obtained in all GBMs and PAs. The mean percentage of HIF-1α–positive cells was 18% in the PAs (14% and 22%) and 63% in the GBMs (55% and 70%) for the 2 observers, respectively.

RNA Expression Arrays

RNA expression patterns of 7 PAs were compared with those of 8 GBMs and 7 normal brain samples (Table 1). Differentially expressed genes between PAs and the GBMs were identified. Cutoff values of false discovery rates of 0.01 or less and a fold change of 1.5 yielded 4,245 records (2,894 genes) (Ingenuity). Generally, 455 genes out of the total of 2,894 differentially expressed genes belonged to pathways involved in cell cycle regulation. There were differences in the utilization of the genes involved in the HIF-1α pathway between PAs and GBMs.

Angiogenesis-Related Gene Expression Patterns

Focusing on angiogenesis-related genes yielded 114 differentially expressed genes (represented by 159 probes) (Ingenuity). In PAs, 41 out of the 114 genes were upregulated versus GBM. The top 10 canonical pathways in which these

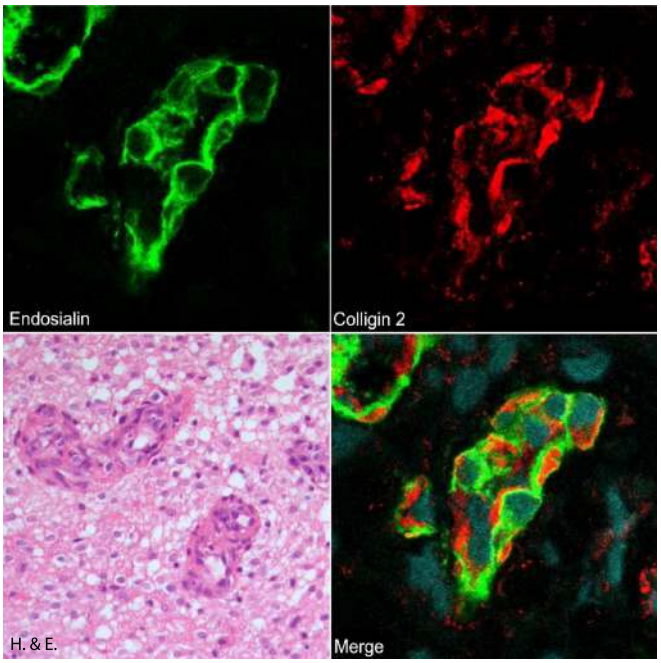

FIGURE 3. Hypertrophic vessels in glioblastoma. The disorganized layering of the vessel wall is illustrated by immunohistochemistry for lumen-lining endosialin-positive cells (lower left panel light microscopy; upper panels and lower right panel confocal microscopy; original magnification = 100×; DAPI counterstain in merged panel lower right). Hematoxylin and eosin stain.

genes take part are shown in Table 4. Most prominently, there were differences in the utilization of molecules taking part in the pathway of hepatic fibrosis/hepatic stellate cell activation, fibroblast growth factor (FGF) signaling, and neuregulin signaling (Table 4). Conversely, 73 out of the 114 angiogenesis-related genes (represented by 105 probes) were upregulated in GBMs versus PAs. The hepatic fibrosis/hepatic stellate cell activation pathway featured most prominently; this was followed by axonal guidance signaling (Table 4). We also looked for genes involved in angiogenesis in embryonic development in the set of genes that were specifically upregulated in PAs and found 32 genes (43 probes). The top 10 canonical pathways are shown in Table 4. There appeared to be a large overlap with the pathways found by only focusing on angiogenesis (Table 4). Filtering for the genes involved in both angiogenesis in embryogenesis that were upregulated in GBM resulted in a list of 64 genes (89 probes). Of the top 10 canonical pathways, the hepatic fibrosis/hepatic stellate cell activation pathway again was prominently featured (Table 4).

DISCUSSION

In the present study, we compared the hypertrophic vasculature of PA and GBM by confocal microscopy to coexpression patterns of vascular cell lineage markers. In addition, we compared the expression profiles of the tumors focusing on angiogenesis-related genes. We found structural differences of the newly formed blood vessels between the glioma subtypes and also differences in the utilization of angiogenic pathways. In contrast to GBMs, the cellular composition of the hypertrophic and glomeruloid blood vessels in PAs generally had organized appearances. In early studies on the vasculature of PAs, it was suggested that endothelial cells would not take part in the cellular proliferation of the vessel walls (25, 26), but specific lineage markers for endothelial cells used in the present study proved the contrary. In the PAs, the pericytes remained in an abluminal position.

Endosialin (initially called ''tumor endothelial marker 1'' [TEM1]) was introduced as a marker for tumor-associated endothelial cells (16, 27, 28) but appeared to be expressed by cells surrounding endothelial cells, also known as mural cells in human neoplasms (15, 16). Although the expression of endosialin in the vasculature of experimental tumors is not restricted to pericytes, we did not find any overlap with endothelial cells in this study. In mouse development, endosialin is expressed by endothelial and fibroblast-like cells (28, 29). The expression in fibroblast-like cells is prominent around buds of developing endothelia as seen in developing kidney and lung (29). In mouse knockouts of endosialin, the development of tumor xenografts is hampered because of maldevelopment of the vasculature (29); this points to a role for endosialin in the interplay among tumor cells, endothelium, and surrounding mesenchymal cells.

In the present study, we also found that expression of NG2 was in all types of GBM blood vessels and in the PA vasculature, although it was more restricted in the latter. NG2 is a transmembrane proteoglycan that serves as a promoter of angiogenesis; it is reportedly expressed in pericytes and stromal cells around newly formed blood vessels (30). The relative preserved position of the pericytic cells in the vessels of the PAs (in contrast to that in GBM) may reflect intact regulation of angiogenesis.

The cellular layering of the vessel walls in PA appears to be regular and organized, and unlike the situation in GBM, the lumina are generally patent. In a recent study, the blood vessels of 59 PAs and 62 GBMs were compared by conventional microscopy, and the diameters of the vessels in PAs were found to be larger than those in GBMs (14). By immunohistochemistry, the authors did not find substantial differences for angiopoietin-1 and -2 and VEGF-A expression between the glioma subtypes (14). The present findings confirm the expression of angiopoietin-1 and -2 and VEGF-A in both PA and GBM, but the expression was more extensive in the latter, suggesting more severe hypoxic conditions in the GBM. In glioma xenografts, the formation of glomeruloid vascular structures appeared to correlate with expression levels of Ang1, and no such structures were formed when its cognate receptor Tie2 was blocked (31). The glomeruloid vessels reflect improperly accelerated angiogenesis resulting in dysfunctional abortive vascular proliferation (32). The differences in expression of αSMA, endosialin, and NG2 may reflect differences in proliferation and recruitment of the cellular constituents of the hypertrophied blood vessels caused by differences in the amounts of the hypoxia-related regulatory factors present and in the contribution of intrinsic tumor type-associated developmental pathways.

The morphologic diversity of glioma blood vessels has been addressed in previous studies (14, 33), but there are

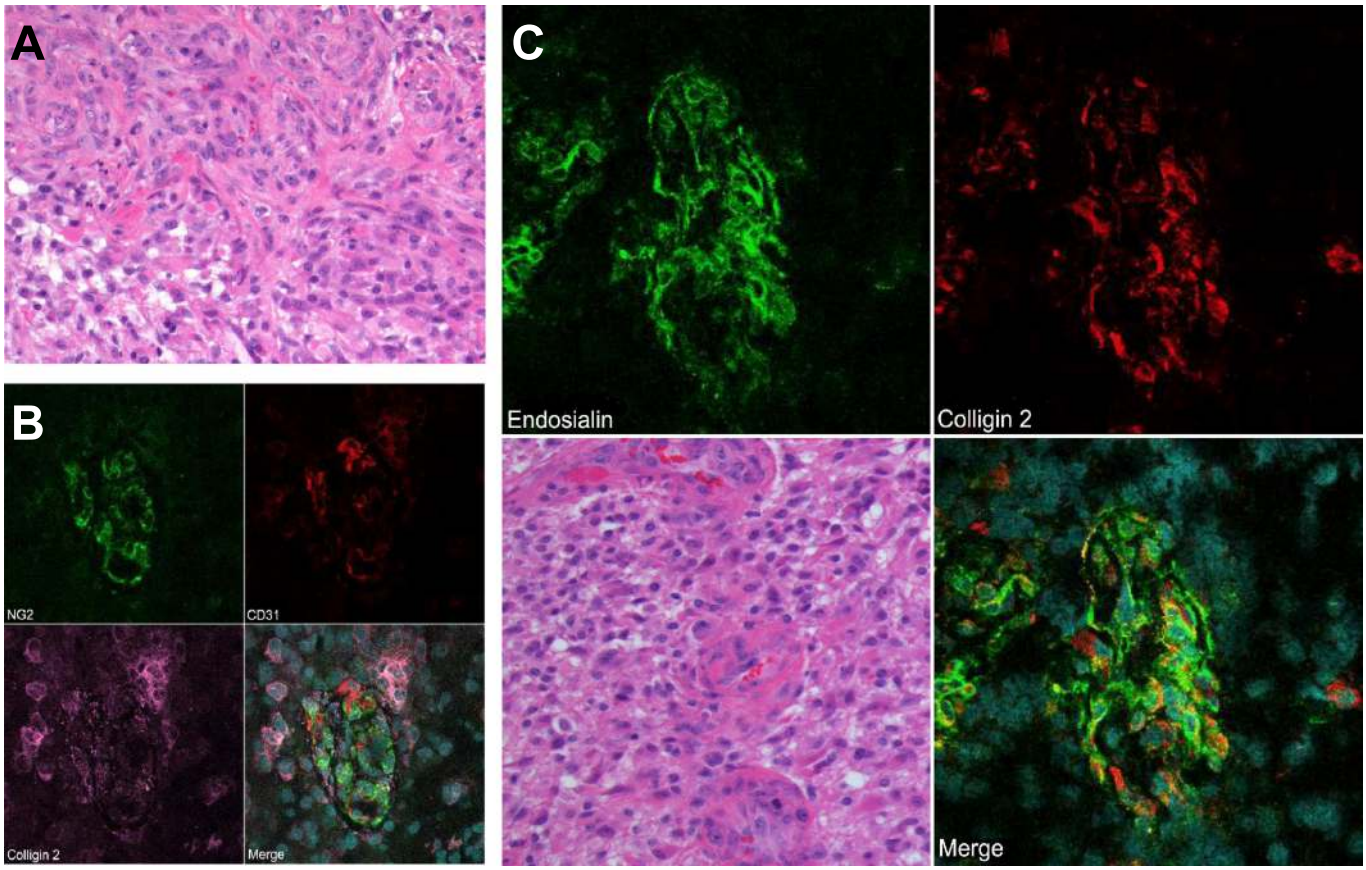

FIGURE 4. Glomeruloid microvascular proliferation in glioblastoma. **(A)** The upper part of this figure shows glomeruloid blood vessels, and the lower left part shows a glial tumor. Lumina of the vessels are obliterated, and no layering is evident (hematoxylin and eosin stain [H&E]; original magnification = 200×). **(B)** Disorganized arrangements of CD31-positive endothelial cells and NG2-positive pericytes (confocal microscopy; original magnification = 200×; DAPI counterstain in merged panel lower right). **(C)** Pericytes stained by endosialin occupy sites throughout the vessel wall and often lining irregular lumina (lower left panel light microscopy H&E; original magnification = 200×); upper panels and lower right panel confocal microscopy; original magnification = 100×; DAPI counterstain in merged panel lower right).

few data on differences in underlying molecular stimuli. The genes that discriminated most between PAs and GBMs seem to be involved in cell cycle regulation; this confirms data in the literature on gene expression in glioma subsets (34–37). Unsupervised analysis of gene expression in glioma subsets revealed tumor lineage (35, 36) and tumor grade (34) as major classifiers. In a study in which PAs and low-grade diffusely infiltrating gliomas were compared for discriminating gene expression patterns, immune system–related genes, genes involved in cell adhesion, migration, and some angiogenesis-related genes were found to be differentially expressed (35). Using higher-order transcriptional network analysis of gene expression data sets to identify gene regulatory pathways specific to various glioma types and grades, Deshmukh et al (38) mainly found differences in transcription factors but no angiogenesis-related genes. Colin et al (37) compared PAs with GBMs using suppression subtractive hybridization to the mRNA of 4 GBMs and 4 PAs and discovered that no more than 5 angiogenesis-related genes were overexpressed in GBM, whereas none were in the PA group. In the present study, we focused on expressional differences of angiogenesis-related genes and pathways and found transcriptional differences. Among the top 10 canonical angiogenesis-related pathways in which differential utilization was demonstrated, the hepatic fibrosis/hepatic stellate cell activation pathway emerged as most prominent. On various external stimuli and proinflammatory events, liver stellate cells secrete cytokines linking to various cascades, among which is the NF-κB pathway. Nuclear factor-κB activation (phosphorylation of IκBα) is involved in lipopolysaccharide/interferon-γ– or interleukin-1β/interferon-γ–induced inducible nitric oxide synthase expression in normal astrocytes (39). The NF-κB pathway is activated in GBM-initiating cells (40, 41) and is activated by Bmi-1 overexpression, triggering glioma angiogenesis in orthotopically transplanted human gliomas (42), offering new targets for antiangiogenic therapy in gliomas. The hepatic fibrosis/hepatic stellate cell activation pathway has never previously been connected to glial neoplasms, but the association between inflammatory response, angiogenesis, and tumor formation is an emerging concept (43). Involvement of the FGF family in glioma genesis and angiogenesis is well known. Recently, activating mutations in 2 hotspots within

TABLE 4. Top 10 Canonical Pathways and Genes Emerging From Comparisons of RNA Expression Between Glioblastomas and Pilocytic Astrocytomas Focusing on Angiogenesis and Embryonic Development

		Upregulated in Pilocytic Astrocytomas		Upregulated in Glioblastomas	
Gene Symbol	**Pathway**	**Angiogenesis**	**Angiogenesis in Embryonic Development**	**Angiogenesis**	**Angiogenesis in Embryonic Development**
FGF2;LEPR;FGFR1;TGFA;TNF;FGF1;BCL2	Hepatic fibrosis / stellate cell activation	7.38E+00*	8.17e+00	6.80E+00	7.25E+00
VEGFA; COL1A1; VCAM1; FN1; PDGFA; TGFB2; ECE1; PGF		4.79E-02†	4.79e-02	5.48E-02	5.48E-02
FGF2;CRKL;PIK3R1;FGFR1;PRKCA;FGF1	FGF signaling	7.10E+00	6.14E+00		
		6.52E-02	5.43E-02		
CRKL;PIK3R1;TGFA;PRKD1;PTEN;PRKCA	Neuregulin signaling	7.01E+00	6.07E+00		
		5.88E-02	4.90E-02		
ABI1;PIK3R1;ITGB5;PRKD1;PRKCA	Macropinocytosis signaling	6.19e+00	5.08E+00		
		6.58e-02	5.26E-02		
PIK3R1;HIPK2;PTEN;BCL2;SIRT1	P53 signaling	5.51E+00	6.07E+00		
		5.21E-02	5.21E-02		
CRKL;PIK3R1;RAP1A;PRKD1;PRKCA	HGF signaling	5.32E+00			
		4.76E-02			
PPARA;PIK3R1;TNF;RAP1A;PRKD1;PRKCA	NO react oxygen species in macrophages	5.24E+00			
		2.86E-02			
PIK3R1;ITGB5;TEK;PRKD1;PRKCA;BCL2	IL-8 signaling	5.22E+00	4.57E+00		
		2.92E-02	2.44E-02		
ITGA9;CRKL;PIK3R1;RAP1A;ITGB5;PTEN	Integrin signaling	5.11E+00	4.48E+00		
		2.90E-02	2.42E-02		
EDIL3;CRKL;PIK3R1;RAP1A;PRKD1;PRKCA	Leukocyte extravasation signaling	5.09E+00			
		2.99E-02			
ITGA9;CRKL;PIK3R1;ITGB5;PTEN;FGFR1;BCL2	PTEN signaling		4.09E+00		
			2.96E-02		
PIK3R1; NCOA1; TNF; PRKD1	IL-12 signaling		3.87E+00		
			2.56E-02		
SEMA3E; ADAMTS8; CRKL; PIK3R1; NTN1; PRKD1	Axonal guidance signaling		3.83+00	6.47E+00	7.13E+00
VEGFA; ADAM17; EPHB4; EPHB2; PDGFA; ITGA2; ITGA5; EPHB3; FZD5; PGF; WNT5A; NRP1			1.28E-02	2.56E-02	2.56E-02
COL1A1; ADAM17; SPP1; JUN; ITGA2; ITGA5; FZD5; SMAD5; CTNNB1; WTN5A	Role of osteoblast			7.38E+00	7.95+00
				4.20E-02	4.20E-02
VEGFA; EPHB4; EPHB2; PDGFA; ACP1; ITGA2; ITGA5EPHB3; PGF	Ephrin receptor signaling			7.15E+00	6.46E+00
				4.48E-02	3.98E-02
VEGFA; VCAM1; FN1; JUN; PDGFA; FZD5; CTNNB1; PGF; WNT5A	Role of macrophages			5.13E+00	5.62E+00
				2.71E-02	2.71E-02
VEGFA; JUN; TGFB2; FZD5; CTNNB1; PGF; BIRC5; WNT5A	Colorectal cancer metastasis signaling			4.97E+00	5.41E+00
				3.10E-02	3.10E-02
VEGFA; FN1; JUN; FLNA1; ITGB8; CTNNB1; PGF	ILK signaling			4.77E+00	5.15E+00
				3.65E-02	3.65E-02
VEGFA; F2R; EPHB2; PDGFA; ITGA5; ITGB8; PGF	Clathrin-mediated endocytosis signaling			4.75E+00	5.13E+00
				3.57E-02	3.57E-02
VEGFA; E2F1; FZD5; CTNNB1; PGF; WNT5A	Ovarian cancer signaling				4.91E+00
					4.23E-02
CXCL10; SPP1; PDGFA; MED1; TGFB2	VDR/RXR activation			4.61E+00	4.89E+00
				6.17E-02	6.17E-02
EPHB4; EPHB2; ACP1; EPHB3; CTNNB1	Ephrin B signaling			4.72E+00	
				6.17E-02	

In the first column, the differentially expressed genes are listed. The gene symbols represent the angiogenesis-related genes of which the expressional levels were found to be significantly different, either upregulated in pilocytic astrocytoma (PA) or in glioblastoma (GBM). Values of p and ratios are listed in columns 3 to 6. In the second column, the pathways in which the genes participate are listed. Some pathways may be present in the list for PA as well as GBM because of significant expressional differences of subsets of participating genes.

*log (p value).

†ratio.

FGF indicates Fibroblast Growth Factor; HGF, Hepatocyte Growth Factor; NO, Nitric Oxide; ILK, integrin Linked Kinase; VDR, vitamin D Receptor; RXR, Retinoid X Receptor.

the kinase domain of FGF receptor 1 (FGFR1) were discovered in some PAs (44), whereas the present study identified upregulation of FGF-2 in the PAs (Table 4). Fibroblast growth factor-2 serves as a proangiogenic factor, and anti-FGF agents have significant effects on tumor growth in vitro (45).

The question of whether specificity of inhibiting agents for the various molecules in angiogenic pathways would show different effects in PA versus GBM remains to be investigated. The results of immunohistochemistry for VEGF-A and HIF-1α (considered as indicators of hypoxia) showed a considerable number of hypoxic cells in the PA samples, corroborating the finding that the VEGF/VEGFR pathway is involved in diffuse astrocytoma as well as in PA. Furthermore, in both glioma subtypes, the hypoxia-driven pathways are active, but there are differences in utilization of the participating molecules. Differences in the utilization of the VEGF pathway have been reported for the 3 malignancy grades of diffusely infiltrating astrocytomas: angiogenic activity of VEGF was correlated with that of insulin-like growth factor binding protein 2 and both molecules seemed to be overexpressed around palisading necrosis while their activity significantly differed between tumors of different malignancy grades (34). So far, there are no data on possible differences between diffuse gliomas and PAs in this regard.

In conclusion, further studies are necessary to link differences in utilization of particular angiogenesis-related pathways to mechanisms of neoangiogenesis and resulting structural abnormalities of the blood vessel walls in PAs and GBMs. Detailed knowledge of aberrant angiogenic processes may lead to defining new targets for effective antiangiogenic therapies for gliomas.

ACKNOWLEDGMENTS

We thank Prof. Clare Isacke and Dr. Nicole Simonavicius from the Institute of Cancer Research, UK, for providing us with the endosialin antibody. We also thank Frank van de Panne for assistance with the photography.

REFERENCES

1. Vredenburgh JJ, Desjardins A, Reardon DA, et al. The addition of bevacizumab to standard radiation therapy and temozolomide followed by bevacizumab, temozolomide, and irinotecan for newly diagnosed glioblastoma. Clin Cancer Res 2011;17:4119–24
2. Gerstner ER, Duda DG, di Tomaso E, et al. Antiangiogenic agents for the treatment of glioblastoma. Exp Opin Investig Drugs 2007;16:1895–908
3. Kaur B, Khwaja FW, Severson EA, et al. Hypoxia and the hypoxia-inducible-factor pathway in glioma growth and angiogenesis. Neuro-Oncology 2005;7:134–53
4. Holash J, Maisonpierre PC, Compton D, et al. Vessel cooption, regression, and growth in tumors mediated by angiopoietins and VEGF. Science 1999; 284:1994–98
5. Holash J, Wiegand SJ, Yancopoulos GD. New model of tumor angiogenesis: Dynamic balance between vessel regression and growth mediated by angiopoietins and VEGF. Oncogene 1999;18:5356–62
6. Leon SP, Folkerth RD, Black PM. Microvessel density is a prognostic indicator for patients with astroglial brain tumors. Cancer 1996;77: 362–72
7. Abramsson A, Berlin O, Papayan H, et al. Analysis of mural cell recruitment to tumor vessels. Circulation 2002;105:112–17
8. Kleihues P, Louis DN, Wiestler OD, et al. WHO grading of tumours of the central nervous system. In: Louis DN, Ohgaki H, Wiestler OD, Cavenee WK eds. WHO Classification of Tumours of the Central Nervous System. Lyon, France: International Agency for Research on Cancer, 2007;10–11
9. Birlik B, Canda S, Ozer E. Tumour vascularity is of prognostic significance in adult, but not paediatric astrocytomas. Neuropathol Appl Neurobiol 2006;32:532–38
10. Fulham MJ, Melisi JW, Nishimiya J, et al. Neuroimaging of juvenile pilocytic astrocytomas: An enigma. Radiology 1993;189:221–25
11. Evans SM, Hahn SM, Magarelli DP, et al. Hypoxic heterogeneity in human tumors: EF5 binding, vasculature, necrosis, and proliferation. Am J Clin Oncol 2001;24:467–72
12. Jones DT, Kocialkowski S, Liu L, et al. Oncogenic RAF1 rearrangement and a novel BRAF mutation as alternatives to KIAA1549:BRAF fusion in activating the MAPK pathway in pilocytic astrocytoma. Oncogene 2009;28:2119–23
13. Zerilli M, Zito G, Martorana A, et al. BRAF(V600E) mutation influences hypoxia-inducible factor-1alpha expression levels in papillary thyroid cancer. Modern Pathol 2010;23:1052–60
14. Sie M, de Bont ES, Scherpen FJ, et al. Tumour vasculature and angiogenic profile of paediatric pilocytic astrocytoma: Is it much different from glioblastoma? Neuropathol Appl Neurobiol 2010;36:636–47
15. Rettig WJ, Garin-Chesa P, Healey JH, et al. Identification of endosialin, a cell surface glycoprotein of vascular endothelial cells in human cancer. Proc Natl Acad Sci U S A 1992;89:10832–36
16. Christian S, Winkler R, Helfrich I, et al. Endosialin (Tem1) is a marker of tumor-associated myofibroblasts and tumor vessel-associated mural cells. Am J Pathol 2008;172:486–94
17. Sugimoto H, Mundel TM, Kieran MW, et al. Identification of fibroblast heterogeneity in the tumor microenvironment. Cancer Biol Ther 2006;5: 1640–46
18. Virgintino D, Girolamo F, Errede M, et al. An intimate interplay between precocious, migrating pericytes and endothelial cells governs human fetal brain angiogenesis. Angiogenesis 2007;10:35–45
19. Simonavicius N, Robertson D, Bax DA, et al. Endosialin (CD248) is a marker of tumor-associated pericytes in high-grade glioma. Modern Pathol 2008;21:308–15
20. Mustafa D, van der Weiden M, Zheng P, et al. Expression sites of colligin 2 in glioma blood vessels. Brain Pathol 2010;20:50–65
21. Mustafa DA, Dekker LJ, Stingl C, et al. A proteome comparison between physiological angiogenesis and angiogenesis in glioblastoma. Molec Cell Proteomics 2012;11:M111 008466
22. Gravendeel LA, Kouwenhoven MC, Gevaert O, et al. Intrinsic gene expression profiles of gliomas are a better predictor of survival than histology. Cancer Res 2009;69:9065–72
23. French PJ, Swagemakers SM, Nagel JH, et al. Gene expression profiles associated with treatment response in oligodendrogliomas. Cancer Res 2005;65:11335–44
24. Schroeder A, Mueller O, Stocker S, et al. The RIN: An RNA integrity number for assigning integrity values to RNA measurements. BMC Molec Biol 2006;7:3
25. Forsyth PA, Shaw EG, Scheithauer BW, et al. Supratentorial pilocytic astrocytomas. A clinicopathologic, prognostic, and flow cytometric study of 51 patients. Cancer 1993;72:1335–42
26. Tomlinson FH, Scheithauer BW, Hayostek CJ, et al. The significance of atypia and histologic malignancy in pilocytic astrocytoma of the cerebellum: A clinicopathologic and flow cytometric study. J Child Neurol 1994;9:301–10
27. Teicher BA. Newer vascular targets: Endosialin (review). Int J Oncol 2007;30:305–12.
28. Tomkowicz B, Rybinski K, Foley B, et al. Interaction of endosialin/TEM1 with extracellular matrix proteins mediates cell adhesion and migration. Proc Natl Acad Sci U S A 2007;104:17965–70
29. Rupp C, Dolznig H, Puri C, et al. Mouse endosialin, a C-type lectin-like cell surface receptor: Expression during embryonic development and induction in experimental cancer neoangiogenesis. Cancer Immun 2006; 6:10
30. Stapor PC, Azimi MS, Ahsan T, et al. An angiogenesis model for investigating multicellular interactions across intact microvascular networks. Am J Physiol Heart Circ Physiol 2013;304:H235–45
31. Zadeh G, Reti R, Koushan K, et al. Regulation of the pathological vasculature of malignant astrocytomas by angiopoietin-1. Neoplasia 2005;7: 1081–90
32. Plate KH. Mechanisms of angiogenesis in the brain. J Neuropathol Exp Neurol 1999;58:313–20

33. Eberhard A, Kahlert S, Goede V, et al. Heterogeneity of angiogenesis and blood vessel maturation in human tumors: Implications for antiangiogenic tumor therapies. Cancer Res 2000;60:1388–93
34. Godard S, Getz G, Delorenzi M, et al. Classification of human astrocytic gliomas on the basis of gene expression: A correlated group of genes with angiogenic activity emerges as a strong predictor of subtypes. Cancer Res 2003;63:6613–25
35. Huang H, Hara A, Homma T, et al. Altered expression of immune defense genes in pilocytic astrocytomas. J Neuropathol Exp Neurol 2005; 64:891–901
36. Li A, Walling J, Ahn S, et al. Unsupervised analysis of transcriptomic profiles reveals six glioma subtypes. Cancer Res 2009;69:2091–99
37. Colin C, Baeza N, Bartoli C, et al. Identification of genes differentially expressed in glioblastoma versus pilocytic astrocytoma using suppression subtractive hybridization. Oncogene 2006;25:2818–26
38. Deshmukh H, Yu J, Shaik J, et al. Identification of transcriptional regulatory networks specific to pilocytic astrocytoma. BMC Med Genomics 2011;4:57
39. Nomura Y. NF-kappaB activation and IkappaB alpha dynamism involved in iNOS and chemokine induction in astroglial cells. Life Sci 2001;68: 1695–701
40. Nogueira L, Ruiz-Ontanon P, Vazquez-Barquero A, et al. The NFkappaB pathway: A therapeutic target in glioblastoma. Oncotarget 2011;2:646–53
41. Atkinson GP, Nozell SE, Benveniste ET. NF-kappaB and STAT3 signaling in glioma: Targets for future therapies. Expert Rev Neurotherapeutics 2010; 10:575–86
42. Jiang L, Song L, Wu J, et al. Bmi-1 promotes glioma angiogenesis by activating NF-kappaB signaling. PloS One 2013;8:e55527
43. Copple BL, Bai S, Burgoon LD, et al. Hypoxia-inducible factor-1alpha regulates the expression of genes in hypoxic hepatic stellate cells important for collagen deposition and angiogenesis. Liver Int 2011;31: 230–44
44. Jones DT, Hutter B, Jager N, et al. Recurrent somatic alterations of FGFR1 and NTRK2 in pilocytic astrocytoma. Nat Gen 2013;45:927–32
45. Jensen RL. Growth factor-mediated angiogenesis in the malignant progression of glial tumors: A review. Surg Neurol 1998;49:189–95

